COO 4094-74

CONF-800106--15

# A COMPARISON OF THEORY AND EXPERIMENT FOR PHOTOVOLTAIC/THERMAL COLLECTOR PERFORMANCE *+++

Susan D. Hendrie
Pattabiraman Raghuraman

Massachusetts Institute of Technology
Lincoln Laboratory
Lexington, Massachusetts 02173



## ABSTRACT

Detailed performance testing of an air and a liquid type combined photovoltaic/thermal (PV/T) collector has been completed with results of accompanying analytical modeling accurately predicting the experimental data. Thermal efficiencies, with concurrent photovoltaic operation at the maximum power point, are computed in accordance with ASHRAE 93-77 specifications and collector-surface heat-transfer coefficients are determined. Analytical modeling of the two collectors from first principals accounts for the non-ideal bonding of photovoltaic cells to the thermal collector components and for the spacing between cells.

## INTRODUCTION

This paper extends previous work (1) at MIT Lincoln Laboratory on air and liquid PV/T collectors. Prior to this time experimentation and analysis of combined PV/T collectors has included some testing of a partially modified solar thermal collector(2) and, an extension of the conventional Hottel Whillier solar thermal collector model accounting for the presence of photovoltaic cells (3).

This paper reports the results of detailed temperature measurements on collector surfaces. Thermal efficiencies, with concurrent electric energy collection, and electrical efficiencies are compared with analytical results for each collector.

The two collectors described each have three principal components: 1) a thermal barrier to prevent excessive heat losses to the ambient air, 2) photovoltaic cells comprising the primary heat absorbing surface, and 3) a flow passage through which a thermal-transfer fluid passes. The air-type collector employs two low-iron glass covers to prevent upward thermal losses and thermal insulation on the sides and bottom to inhibit backward and edge losses. Photovoltaic cells are bonded to the underside of the innermost cover glass. The photovoltaic cells act as the primary heat-absorbing surface with incident radiation passing between the cells absorbed by a secondary black aluminum absorber plate. The thermal-transfer fluid, air, circulates between the cells and the secondary absorber plate, as shown in Figure 1.

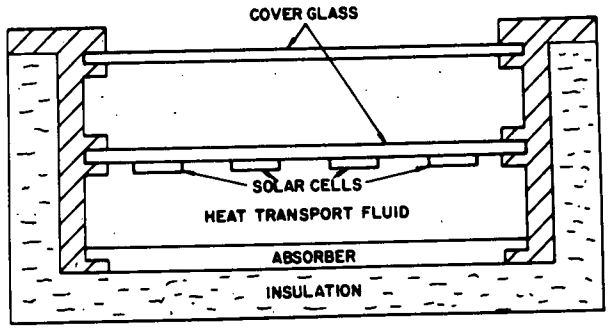


Figure 1. Air PV/T Collector

* This work was sponsored by the U.S. Department of Energy.
+ Presented at the 14th IEEE Photovoltaic Specialists Conference, San Diego, CA 7-10 January 1980.
++ The U.S. Government assumes no responsibility for the information presented.

## DISCLAIMER

The liquid collector utilizes a single glass cover, to prevent upward heat losses, with thermal insulation on the sides and bottom to prevent back and edge losses. Below the glass cover, photovoltaic cells form the primary absorbing surface, with a black aluminum plate placed directly below the cells to absorb insolation passing between them. Copper tubes bonded to the underside of the aluminum plate transport the circulating thermal-transfer fluid, as shown in Figure 2.

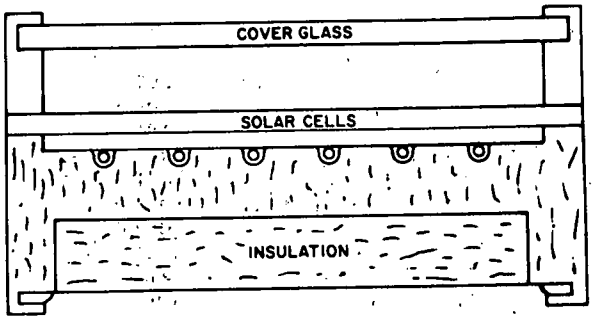


Figure 2. Liquid PV/T Collector

Both collectors were tested outdoors under varying inlet fluid temperature and climactic conditions. Thermal efficiency values were computed, following ASHRAE 93-77 test requirements, with the important addition of concurrent photovoltaic operation at the maximum power point. As efficiency values were recorded, collector surface temperatures were also measured on the cover glass(es), cells, secondary absorber plate and flow passages of each collector. From the surface temperature measurements, important heat-transfer parameters were computed and design improvement recommendations made.

## EXPERIMENTAL APPARATUS

To obtain the desired temperature measurements, each collector was disassembled and fine-gauge copper-constantan thermocouples placed on principal surfaces along the collector length and width, as shown in Figures 3a and 3b. Collectors were then resealed, with additional insulation on the sides and bottom to prevent any possible thermal leaks, and placed on variable-tilt test stands outdoors. Each collector was interfaced with its own distinct flow loop from which fluid temperature and flow conditions were controlled and recorded.

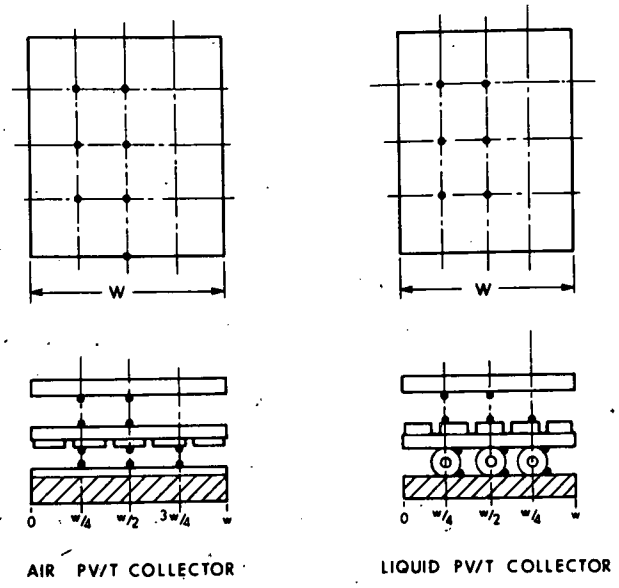


Placement of Thermocouples
Figure 3a. Figure 3b.

The air collector loop is open-ended, drawing air from the atmosphere through variable-temperature heaters into 6-inch insulated ducting leading to the collector inlet. Heated air leaves the collector via identical ducting and, is then dumped into the atmosphere. The liquid collector loop is closed, employing a 60-gallon storage tank from which liquid is drawn through a variable-temperature heater into 1/2-inch diameter piping to the collector. Heated liquid leaving the collector is returned to the tank. Due to the low winter ambient temperatures in Boston, propylene glycol, ($C_p$ = 2.47 kJ/kg°C), was used instead of water as the liquid transfer fluid.

Fluid flow rate was determined using a turbine flow meter upstream of the collector for the liquid collector loop. For the air collector loop, a calibrated nozzle, placed sufficiently far downstream from the collector outlet to ensure a mixed and uniform flow, was used.

Environmental conditions were recorded close to the collector stands, with measurement of ambient temperature, wind speed, wind direction, and total tilted and horizontal direct beam insolation.

During testing, an impedance-matching device was used to ensure that each collector was operating with continuous photovoltaic power output at the maximum power point. Electrical power production was recorded with measurement of collector current, voltage and their instantaneous product.

Following ASHRAE 93-77 specifications, the inlet and outlet temperatures of each collector were also measured by placing copper-constantan thermocouples upstream and downstream of the actual collector inlet and outlet ports, respectively. Although duct and piping from the ports to the measurement point were heavily insulated, some thermal losses along this path were detected in the cold ambient temperatures over which testing was done. In the cases where a greater than 2% error was introduced into the temperature measurements, data were corrected for this loss and the correction noted in results presented.

## TEST PROCEDURE

Throughout the testing, collectors were operated with photovoltaic electrical power output at the maximum power point and with a constant mass flow rate as specified in the ASHRAE 93-77 standards. For the air collector the operating mass flow rate was 0.01m·s$^{-1}$ of standard air (0.18 kg/sec), and for the liquid collector, this value was 0.02kg·m$^{-2}$·s$^{-1}$ (0.035 kg/sec). For each collector, the fluid inlet temperature was varied from a value equal to the ambient temperature up to 60°C. Tests were conducted at varying climactic conditions within the constraints imposed by ASHRAE 93-77: an approximately constant insolation level of at least 0.63 kW/m$^2$ and approximately constant wind conditions and ambient temperature (4). Data were sampled and recorded every minute for discrete time periods equivalent in length to the collector time constant (18.3 minutes for the air collector and 10.8 minutes for the liquid collector). Efficiency values were computed and then integrated over each time period to yield one thermal and one efficiency value per period. Similarly, recorded surface temperature values were averaged over each time period to yield a single value for each measured surface position per time period.

The thermal and electrical efficiencies, defined as per ASHRAE 93-77 are:

$$\eta_t = \frac{\dot{m} c_p \int_{t1}^{t2} (T_{f,o}(t) - T_{f,i}(t))\,dt}{A \int_{t1}^{t2} I\,dt}$$

$$\eta_e = \frac{\int_{t1}^{t2} p\,dt}{A \int_{t1}^{t2} I\,dt}$$

$\dot{m}$ = mass flow rate
A = overall collector area
$C_p$ = Specific heat
$T_{f,i}$ = inlet temperature of fluid
$T_{f,o}$ = outlet temperature of fluid
$I_t$ = total tilted insolation
p = power output

## RESULTS

Figures 4 and 5 show thermal efficiency curves for thermal operation with photovoltaic energy collection at the maximum power point, computed from experimental data and from analytical models. It should be noted that these efficiency values are normalized to the overall collector area, which is in each case approximately 20% larger than the absorbing surface area. The maximum thermal efficiencies, as shown by the curves, are 32.1% for the air collector and 42.6% for the liquid collector. Computed from the curves, the thermal loss coefficient and efficiency factor for each collector is 7.20 W/m$^2$C, and 0.46 for the air collector, 6.77 W/m$^2$C and 0.62 for the liquid collector, respectively (see Tables 1 and 2). The transmission absorption products, also derived from the curves were 0.74 for the air and 0.83 for the liquid collector. The efficiency factor and loss-coefficient values are improved over those previously reported for the same two collectors (1) principally due to the discovery of a heat-loss path in the experimental apparatus which has been corrected in these results. An average thermal loss coefficient for each collector has also been computed from direct temperature measurements, on the cells and in the ambient air. These computed values are cited in Table 2 along with analytically derived average loss-coefficient values.

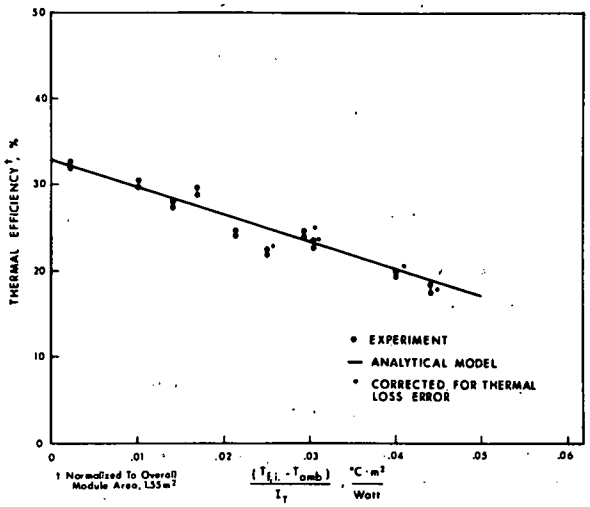


AIR PV/T COLLECTOR THERMAL EFFICIENCY WITH ELECTRICAL ENERGY COLLECTION

Figure 4.

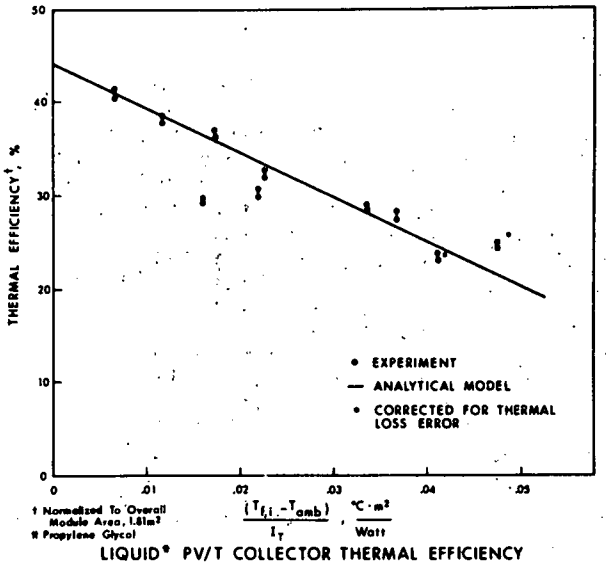


LIQUID# PV/T COLLECTOR THERMAL EFFICIENCY WITH ELECTRICAL ENERGY COLLECTION

Figure 5.

TABLE 1

SUMMARY OF COLLECTOR SPECIFICATIONS

| | Overall Area, m² | Aperture Area, m² | Absorber Area, m² | Cell Packing Factor, % | Cell $\eta_E$,% | Collector $\eta_T$ Max | Collector $\eta_E$ Max |
|---|---|---|---|---|---|---|---|
| Air PV/T | 1.55 | 1.46 | 1.26 | .63 | 11.8 @ 45°C | 32.1* | 6.2* |
| | | | | | | 32.0° | 6.6° |
| Liquid PV/T | 1.81 | 1.60 | 1.48 | .83 | 10.7 @ 28°C | 42.6* | 6.6* |
| | | | | | | 43.5° | 6.7° |

* Experimental Measurement
° Analytical Model

TABLE 2

COMPUTED HEAT TRANSFER COEFFICIENTS + #

| Air PV/T Collector | Experimental | Analysis |
|---|---|---|
| $U_L$ | 7.20 | 7.2 |
| $F_R$ | 0.46 | 0.44 |
| $\tau\alpha$ | 0.74 | 0.74 |
| $H_{CELLS-FLUID + ABSORBER}$ | 6.12 | 6.0 |
| $H_{CELL-FRAME\ EDGE}$ | 3.53 | ---- |
| $H_{CELL-BOTTOM\ FRAME}$ | 2.74 | ---- |
| **Liquid PV/T Collector** | | |
| $U_L$ | 6.77 | 7.2 |
| $F_R$ | 0.62 | 0.58 |
| $\tau\alpha$ | 0.83 | 0.77 |
| $H_{CELLS-ABSORBER}$ | 24.9 | 40. |
| $H_{CELLS-TUBE\ WALL}$ | 23.6 | ---- |
| $H_{ABSORBER-TUBE\ WALL}$ | 204. | ---- |
| $H_{CELLS-FRAME\ EDGE}$ | ---- | ---- |
| $H_{CELLS-FRAME\ BOTTOM}$ | 7.69 | ---- |

+ Averaged over $T_{F,IN}$ = 20 - 40°C and ambient conditions described in Table 1.
# Watts/m²°C

## SUMMARY OF TEST CONDITIONS

| | |
|---|---|
| Ambient Temperature | 1.4 - 1 6. |
| Insolation, ( kW/m$^2$) | .64 - .95 |
| Wind Speed, (m/sec) | 2.3 - 4.9 |
| Fluid Inlet Temperature (°C) | 1.4 - 60 |
| Fluid Flow Rate (kg/sec) | .018 (Air PV/T,) |
| | .035 (Liq. PV/T) |

The electrical efficiency curves generated from experimental data and analysis are shown in Figure 6. Again, efficiency values are normalized to the overall collector area. Maximum electrical efficiencies as shown by the curves are 6.2% for the air collector and 6.6% for the liquid collector. The curves show, as expected, a decreasing cell efficiency with increasing fluid temperature.

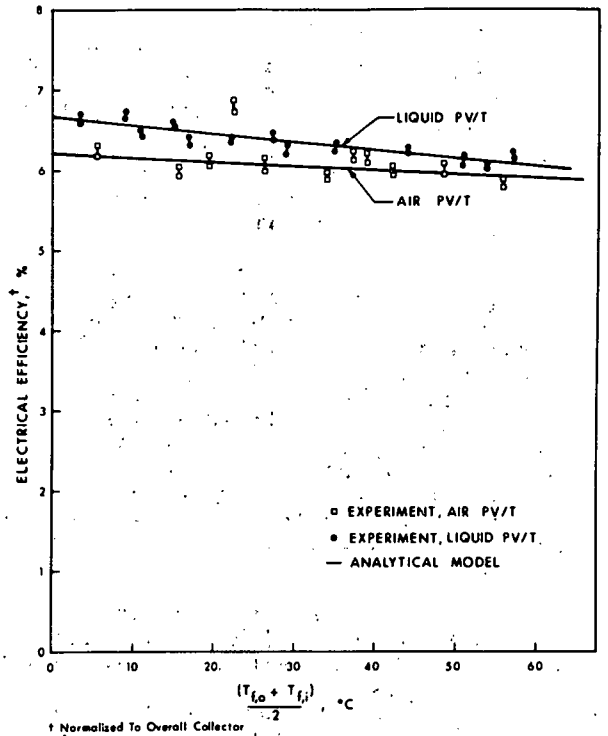


ELECTRICAL EFFICIENCY vs AVERAGE FLUID TEMPERATURE

Figure 6.

Curves typical of surface-temperature measurement results across the width of each collector, measured halfway down the collector length, are shown in Figures 7 and 8. For both collectors, in all test cases, an increasing temperature was observed moving across the collector width from the center to the edges. Looking at the two collector cross-section geometries shown in Figures 1,2, one notices that the steep frame borders abutting the top glass could easily create recirculation regions along the glass edges, making them immune to the forced convective cooling by the wind, to which the rest of the glass sheet is subjected. The inner glass, cells and absorber plate also see a temperature increase from the center to the edges. Here, however, the inhibited cooling mechanism at the edges is forced and natural convection. On these surfaces this center-to-edge temperature differential becomes less pronounced along the flow length. This may be ascribed in part to increased fluid temperature along the flow length and, therefore, a lower heat transfer to the fluid from the cell and absorber surfaces. For this same reason, we find an increasing cell and absorber temperature along the flow, as shown in Figures 9,10. Comparing the cell surface-temperature curves for the two collectors, one notes that the cell temperatures are lower in the liquid collector than in the air. This is a result principally of lower liquid-collector-cell heating due to lower cover-glass transmissivity, coupled with the increased heat-absorbing potential of the liquid as a transfer fluid, compared to air. Despite the difference in fluid temperature and ambient conditions under which the air and liquid collector temperature measurements shown in Figures 9 and 10 were made, when transmission, thermal loss and heating considerations are applied, the effective cell surface heating of both collectors is in each case approximately equivalent, hence the two curves can be directly compared.

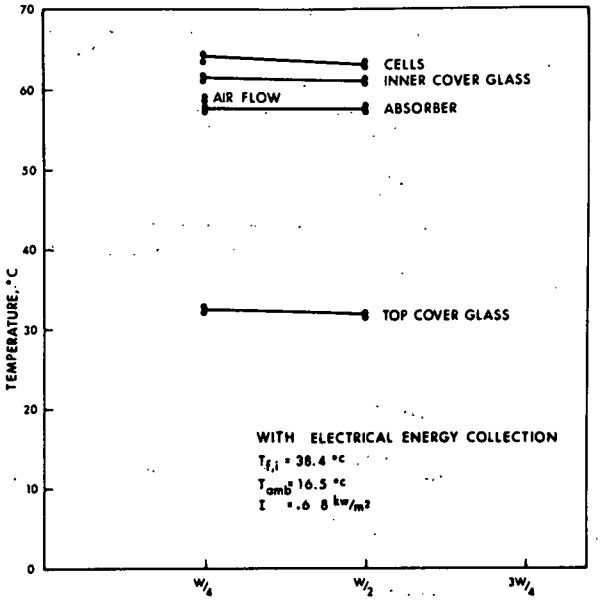


VARIATION OF SURFACE TEMPERATURE† ACROSS AIR PV/T COLLECTOR WIDTH

Figure 7.

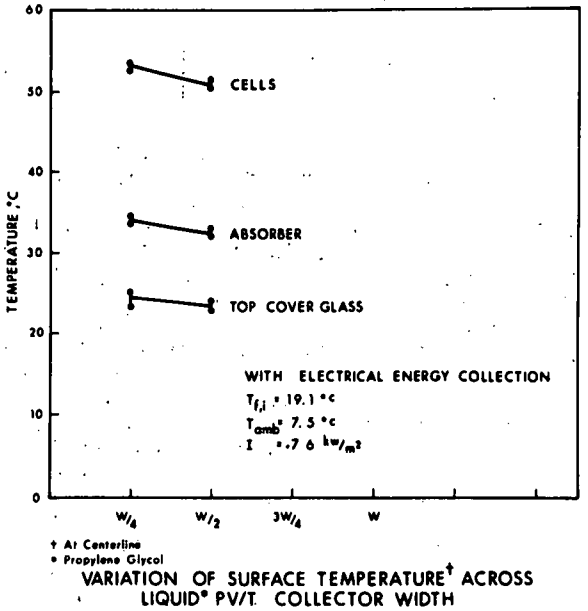


VARIATION OF SURFACE TEMPERATURE† ACROSS LIQUID* PV/T COLLECTOR WIDTH

Figure 8.

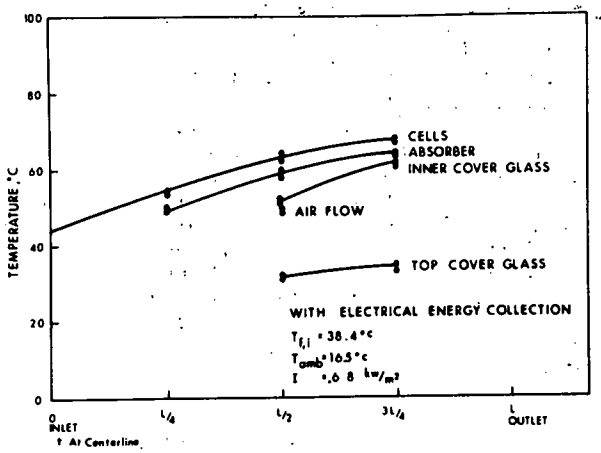


VARIATION OF SURFACE TEMPERATURE† ALONG AIR PV T COLLECTOR LENGTH

Figure 9.

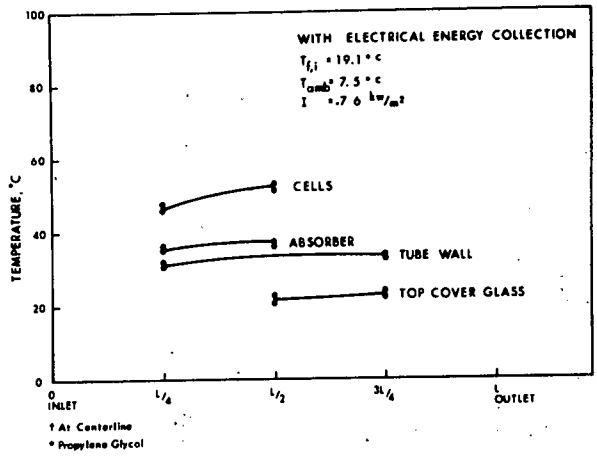


VARIATION OF SURFACE TEMPERATURE† ALONG LIQUID* PV/T COLLECTOR LENGTH

Figure 10.

Air collector curves, shown in Figure 9, indicate a poor cell-to-fluid conductivity with a temperature gradient of 17°C between the two, at an inlet fluid temperature of 38.4°C and under the test conditions cited. The absorber plate-to-fluid conductivity was much better, with a temperature gradient of 4°C. This result is as expected, since the fluid is in direct contact with the absorber surface, unlike the cell-to-fluid interface. The inner cover-glass temperature, as expected, follows that of the cells along the collector length. The inner glass temperature is hotter than that of the absorber plate due to its closer proximity to the primary heat-absorbing surface, the cells. The glass is separated from the cells by only the cell-to-glass bonding material, whereas the absorber is separated from the cells by the cell encapsulant and moving air-transfer fluid. Absorber-plate heating is much less than the cell heating, differing in temperature from the cells by 13°C. The top cover-glass temperatures are 40-50% lower than those of the other collector surfaces due to the direct exposure of this surface to the ambient air.

Figure 10 shows liquid collector-surface temperature variation along the collector length, again measured along the collector centerline. The lower cell temperature shown here is due, as mentioned, to the increased heat-absorbing capability of the liquid-transfer fluid versus air and to the lower cover-glass transmissivity. A comparision of the cell and absorber-plate curves indicates a poor thermal-bond conductivity between these surfaces, yielding a temperature differential of 11.4°C between the two.

The absorber plate to tube thermal conductivity is good, with a temperature gradient of 2.5°C between these two surfaces. The top cover-glass temperature curve is again much lower than the other surface-temperature curves due to direct contact of the top glass with the cold ambient air. The heat-transfer coefficients computed from this and additional experimental data are cited in Table 2, with their analytically derived values also listed.

## DISCUSSION

Experimental measurements and analytical modeling from first principals have provided a basis for the understanding of air and liquid-combined PV/T collector energy flows. The analytical results presented were generated from two PV/T collector modules(5), (6). Each model parallels the theoretical development of the Hottel and Whillier collector model departing, however, in several important basic assumptions, which allow for versatility in predicting the performance of specific PV/T collectors, such as the two studied in this paper. In the liquid collector model, analytical work gives consideration to the thermal resistance between the cell surface and the absorber plate on which the cells are fixed. Based on temperature gradients of 11.4°C measured between these two surfaces for the cited test conditions and typical of all others, this assumption is warranted. The air collector model employed allows for a cell-to-absorber plate temperature gradient, with the inclusion of a variable cell-packing factor. Both models apply the energy equation at every component interface, yielding a numerically solvable system of algebraic equations. Outputs

from the models are the computed collector loss coefficients and the thermal and electrical efficiencies.

## CONCLUSION

A summary of computed heat transfer coefficients listed in Table 2 indicates that for each collector, significant performance improvements can be made. In the air PV/T collector, one notes a low cell-to-fluid conductivity and, in the liquid PV/T collector, low cell-to-absorber and cell-to-tube wall conductivities. In the process of disassembling the collectors, it was found that all of these heat flow paths could be greatly enhanced by more careful cell-back-surface encapsulation and surface-bonding techniques. The air-collector back-cell-surface encapsulation was found to have large undulations, of peak height .25 cm. These peaks and their corresponding valleys decrease the effective heat-transfer area to the fluid, creating small recirculation zones. A thin, uniform encapsulation layer, with a slight roughness to promote transfer fluid turbulence, would greatly improve heat transfer. The encapsulation material used, a silicone derivative, could be replaced by an encapsulant of higher thermal conductivity. However, this is not the primary cause of the high thermal resistance computed here.

Upon disassembly of the liquid collector, a spotted and uneven cell-to-absorber bonding was found, creating the poor thermal transfer between these surfaces born out by the thermal conductivity computation. Again, a carefully applied, thin, uniform bonding layer would greatly improve heat transfer here. Uniform application of bond material, as in the case of the air-collector encapsulant, is not an easy task due to overhanging cell interconnection wires and spacing between cells. However, as future PV/T collector cell designs are evolved, this problem will hopefully be remedied by more closely packed and sophisticated cell designs.

For each collector, the computed thermal loss coefficient and transmission-absorption product, Table 2, indicate another performance improvement area. For both collectors, the loss coefficients would be lowered by a higher cell-packing factor and higher cell-to-fluid conductivity. The transmission-absorption products could be improved with, again, a higher cell-packing factor, particularly in the air collector case, and also by higher glass cell-encapsulant transmissivity and higher cell absorptance.

Examining the cell-to-frame edge and cell-to-frame bottom heat-transfer coefficients, the insulation on both collectors is seen to be adequate. A thermal insulating material was used in both cases, of thickness .02m on the edges and .05m on the bottom, below the flow channel(s).

From the results of experiment and analysis, air and liquid combined photovoltaic/thermal collector are seen to have at least three primary areas where significant performance improvements can be made. Similarly, collector electrical efficiency is seen to have several clearly definable performance improvement areas: an improved cell efficiency, increased cell-packing density, and improved glass/encapsulant transmissivity. With the incorporation of these and other design recommendations such as careful choice of cover glass spacing and inducement of turbulent flow in the transfer fluid, the potential for competitive energy collection efficiencies is very promising.

## REFERENCES


1. Hendrie, S.D., "Evaluation of Combined Photovoltaic/Thermal Collectors," ISES 1979 International Congress & Silver Jubilee, Atlanta, 28 May-1 June 1979. COO 4577-8.

2. Smith, D.R. Biringer, K.L. Pritchard, D.A., "Combined Photovoltaic Thermal Collector Testing," Sandia Laboratories, Albuquerque, New Mexico.

3. Florschuetz, L.W., "Extension of Hottel-Whillier Bliss Model to Analysis of Combined Photovoltaic/Thermal Flat Plate Collectors," ISES Solar Energy Society Meeting, Winnipeg, Canada, 15-20 August 1978.

4. "Methods of Testing to Determine the Thermal Performance of Solar Collectors," ASHRAE Standard 93-77, 345 East 47th Street, N.Y. (1977).

5. Raghuraman, P., "Analytical Prediction of the Performance of Spectrolab Photovoltaic/Thermal Flat Plate Collectors," report to be published.

6. Raghuraman, P., "Analytical Prediction of the Performance of the Arco Solar Liquid Photovoltaic/Thermal Flat Plate Collectors," report to be published.